Remote sensing image matching based on non-subsampled contourlet transform and speed up robust features

WU Yiquan[1,2,3], SHEN Yi[1], TAO Feixiang[1]

1. *College of Electronic and Information Engineering, Nanjing University of Aeronautics and Astronautics, Nanjing* 210016, *China*;
2. *Key Laboratory of Agricultural Information Technology, Ministry of Agriculture, Beijing* 100081, *China*;
3. *Jiangxi Province Key Lab for Digital Land, East China Institute of Technology, Nanchang* 330013, *China*

Abstract: Speed Up Robust Features (SURF) is an improvement of Scale Invariant Feature Transform (SIFT). When it is used to match remote sensing images, SURF can significantly increase matching speed, but slightly decrease matching accuracy. Thus, a remote sensing image matching method based on Non-Subsampled Contourlet Transform (NSCT) and SURF is proposed in this paper. First, the remote sensing image to be matched and the reference image are decomposed by NSCT. Two corresponding low-frequency images are obtained. Then, to reduce the influence of high-frequency noise on matching results, two low-frequency images are inputted to the SURF algorithm to obtain pre-matching results. Finally, to solve the error matching problem of the SURF algorithm, the parameters of the transform model are solved by pre-matching results, and the mismatching is eliminated by using the random sample consensus algorithm. A large number of experiments were conducted, and the results show that compared with the SIFT and SURF algorithms, the proposed algorithm improves the matching speed, as well as the matching accuracy, and exhibits good performance in terms of resisting rotation, noise, and brightness changes.

Key words: remote sensing image matching, Scale Invariant Feature Transform (SIFT), Speed Up Robust Features (SURF), Non-Subsampled Contourlet Transform (NSCT)

CLC number: TP751.1 **Document code:** A

Citation format: Wu Y Q, Shen Y and Tao F X. 2014. Remote sensing image matching based on non-subsampled contourlet transform and speed up robust features. Journal of Remote Sensing, 18(3): 618-629 [DOI: 10.11834/jrs.20143113]

1 INTRODUCTION

Image matching refers to comparisons among two or more images to identify their common scenery or to search for the corresponding specific target in the unknown target image according to the known target image. This method is widely used in computer vision, medical image analysis, aircraft cruising guidance, and other fields. In remote sensing image processing, one of the most important applications of image matching is remote sensing image registration. Image registration is a basic pre-processing step of change detection and image fusion. Registration accuracy has an important influence on subsequent data processing. Considerable research has been conducted on image matching. Existing image matching algorithms can be roughly divided into two categories: gray level-based matching and feature-based matching. Feature-based matching includes point (Dufournaud, et al., 2004; Wu, et al., 2006; Wang & Zhao, 2011), line (Bouchafa & Zavidoviqu, 2006; Zhang, et al., 2007), area (Xue, et al., 2006; Liu & Wang, 2007), and other features (Wu, et al., 2002). Remote sensing images of the same scene may exhibit significant differences in gray level because of the difference in shooting time and shooting environment. Therefore, gray level-based matching algorithms cannot obtain good effects and are significantly influenced by noise. Feature-based matching algorithms can be achieved by extracting the common features between two images, which can reduce the influence of noise in the process of feature extraction. Such algorithms are more suitable for remote sensing image matching. Lowe (2004) summarized the existing feature-detection algorithms based on the invariant technique and formally proposed a Scale Invariant Feature Transform (SIFT) algorithm in 1999. The SIFT operator based on scale space remains unchanged despite image rotation, scaling, and affine transform, which is widely used in remote sensing image matching (Li, et al., 2006; Liu, et al., 2008; Li, et al., 2009; Liu, et al., 2011; Zhu, et al., 2011). To suppress high-frequency noise, Liang, et al. (2011) combined multi-resolution analysis with the SIFT algorithm, which improved computing speed and matching accuracy to a certain extent. However, the high dimensional descriptors of SIFT algorithm, as well as its slow speed in detection and

Received: 2013-05-09; **Accepted:** 2013-11-08; **Version of record first published:** 2013-11-15

Foundation: National Natural Science Foundation of China (No. 60872065); Key Laboratory of Agricultural Information Technology, Ministry of Agriculture (No. 2013001); Jiangxi Province Key Laboratory for Digital Land, East China Institute of Technology (No. DLLJ201113)

First author biography: WU Yiquan (1963—), male, professor. His research interests are remote sensing image processing/ analysis/understanding, target detection and tracking, and signal processing. He has published more than 200 papers. E-mail: nuaaimage@163.com

matching, sensitivity to the changes in the viewing angle, and other shortcomings, the high demands of real-time situations cannot be met. PCA-SIFT (Ke & S ukthankar, 2004), GLOH (Mikolajczyk & Schmid, 2005), and other improved algorithms were proposed, but the effect is not i deal. Drawing on the idea of approximate simplification of the SIFT algorithm, Bay, et al. (2008) introduced the integral image and approximately simplified the Gaussian second-order differential template. Then, in 2006, he proposed the Speeded Up R obust Features (SURF) algorithm. Compared with the SIFT a lgorithm, SURF is approximately three times faster, but has more false matching points.

According to the above analysis, considering the advantages of the SURF algorithm in speed and its disadvantage of more false matching points, a remote sensing image matching method based on Non-Subsampled Contourlet Transform (NSCT) and SURF is proposed. The remote sensing image to be matched and the reference image are first decomposed by NSCT. Two corresponding low-frequency images that contain considerable original image information are obtained. Then, to reduce the i nfluence of high-frequency noise on matching results, two low-frequency images are input into SURF algorithm to pre-match. Transform model parameters are then solved according to the matching results. False matching point pairs that exist in p re-matching results are then removed by using the Random Sample Consensus (RANSAC) algorithm. Finally, various anti-interference capabilities of the algorithms are comprehensively analyzed, and the superiority of the proposed algorithm is verified through a comparison with the SIFT and SURF algorithms through experiments.

2 NSCT

Contourlet transform uses pyramidal direction filter bank to decompose an image, and its process can be divided into two s tages: sub-band decomposition and directional transform. In the sub-band decomposition stage, each layer of low-frequency c omponent is decomposed into a low-frequency component and a high-frequency component using Laplacian pyramidal decomposition. In the directional transform stage, direction filter banks are used to decompose the high-frequency component into 2^i (i is a positive integer) directional sub-bands. Thus, the multi-scale decomposition and multi-direction decomposition of an image can be achieved. However, the down-sampling process in contourlet decomposition reduces the redundancy of coefficient with no translation invariance. The ringing artifact will be produced in image processing results. When implementing contourlet transform, the bandwidths of analysis and synthesis filters are both greater than $\pi/2$, which do not meet the sampling theorem and result in spectrum aliasing in the low- and high-frequency c omponents. NSCT (Cunha, et al., 2006), which consists of Non-Subsampled Pyramid (NSP) decomposition and Non-Subsampled Directional Filter Banks (NSDFB), can solve this problem. For each layer, the low-frequency component in the last layer is d ecomposed into a high-frequency and a low-frequency component by NSP. Then, the high-frequency component is decomposed into multiple directional sub-bands by NSDFB. The schematic diagram of NSCT decomposition is shown in Fig. 1.

The differences between NSCT and contourlet transform are as follows. NSCT eliminates spectrum aliasing of contourlet transform. The signal components decomposed by NSP and NSDFB do not use the down-sampling after analysis filter and up-s ampling before synthesis filter, but up-sampling is performed for the corresponding filter. The analysis filtering and synthesis filtering will then be performed for the signal. Therefore, NSCT not only has characteristics, such as multi-scale, locality, and multiple directions, but also has the characteristics of translation invariance and similar sizes for all the sub-band images.

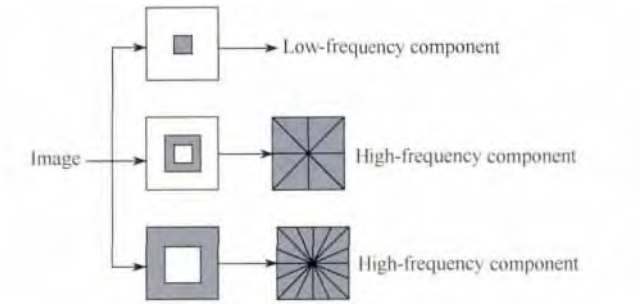

Fig. 1 Schematic diagram of NSCT decomposition

3 SURF ALGORITHM

The SURF algorithm is an improved version of the SIFT a lgorithm with robustness to scale change and rotation and higher speed. This algorithm includes three parts: feature point detection, feature point description, and feature point matching.

3.1 Feature point detection

The SIFT algorithm obtains the next layer image by down-sampling the previous layer image. Then, the next layer image convolves with the Gaussian kernel of different scales. Differences of adjacent layers provide the Difference of Gaussians (DoG) space. Finally, feature points are detected by i dentifying the local extreme value points of the DoG space. To improve speed, the SURF algorithm uses a box filter to approximate the Gaussian filter instead of down-sampling the image. Then, the response function of Hessian matrix determinant is o btained by increasing the box filter template and the integral image. Feature points are calculated on the response function by using the non-maximum inhibition method.

For a certain point $X(x,y)$ in the image I, a Hessian matrix at scale σ in point X is defined as:

$$\boldsymbol{H}(X,\sigma) = \begin{bmatrix} L_{xx}(X,\sigma) & L_{xy}(X,\sigma) \\ L_{xy}(X,\sigma) & L_{yy}(X,\sigma) \end{bmatrix} \quad (1)$$

where $L_{xx}(X,\sigma)$, $L_{xy}(X,\sigma)$, and $L_{yy}(X,\sigma)$ represent the convolution of Gaussian second-order derivative with the image in point X.

Bay, et al. (2008) used a box filter to approximate Gaussian filter. The computation of convolution process is unrelated to filter size, as shown in Fig. 2. The approximation process of the Hessian matrix determinant is shown in Eq. (2).

$$\mathrm{Det}(\boldsymbol{H}) = L_{xx}L_{yy} - L_{xy}^2 = D_{xx}D_{yy} - (0.9D_{xy})^2 \quad (2)$$

where D_{xx}, D_{yy}, and D_{xy} represent the convolution results of a pproximated template in Fig. 2 with image. The value 0.9 is a

weight coefficient that is mainly for balancing the approximation error. It has no significant effect on experimental results.

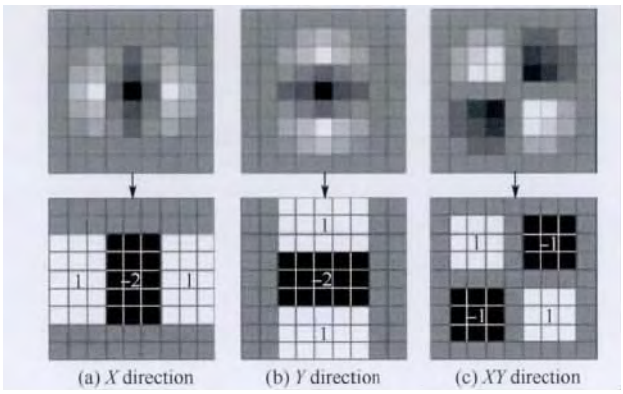

Fig. 2 Approximation of the Gaussian second-order derivative

The image convolution operations are completed by using integral image to improve computational speed further. Integral image $I_\Sigma(X)$ is defined as the sum of pixel values within the rectangular area, which is formed by point X and the origin of image as diagonal vertices,

$$I_\Sigma(X) = \sum_{i=0}^{x}\sum_{j=0}^{y} I(i,j) \tag{3}$$

When computing for the integral image, the original image is only traversed once with a small amount of calculation.

3.2 Feature point description

SIFT uses the gradient information of feature point neighborhood to describe the feature points, whereas SURF uses the gray information of feature point neighborhood. By calculating the first-order Haar wavelet response of integral image, grayscale distribution information is obtained to generate the description vector of feature points.

Step 1 Distribution of main direction. Coefficients of Haar wavelet response are calculated in the x and y directions within a circular neighborhood of 6σ radius around the feature point (σ is the scale at which the feature point is detected). Then, response values within the scope of 60° are summed up to form a new vector. The direction of the longest vector as the main direction of feature point is selected after the entire circular area is traversed.

Step 2 Generation of eigenvectors. The coordinate axis is rotated into the main direction of feature point to ensure rotation invariance. The square region within the range of 20σ is regularly split into smaller 4×4 square sub-regions. Haar wavelet responses are computed at 5×5 regularly spaced sample points for each sub-region. dx is assumed to represent Haar wavelet response in horizontal direction and dy represents Haar wavelet response in vertical direction. Each sub-region can be described as $\boldsymbol{v} = \left[\sum dx, \sum dy, \sum |dy|, \sum |dy|\right]$. All these vectors of sub-regions are concatenated to obtain a descriptor vector length of 64 dimensions.

3.3 Feature point matching

Commonly used feature matching algorithm: for a feature vector, the distances between the vector and all feature vectors of other image are first calculated. Then, the ratios of the nearest neighbor to second nearest neighbor are calculated. If the ratios are less than the preset threshold, the nearest neighbor is considered a good match.

4 ALGORITHMIC PRINCIPLE OF REMOTE SENSING IMAGE MATCHING BASED ON NSCT AND SURF

Although the SURF algorithm can significantly improve the computational speed of the SIFT algorithm, it has a large number of wrong matching point pairs. To solve this problem, a remote sensing image matching algorithm based on NSCT and SURF is proposed to improve matching performance from both the input and output aspects. In terms of input aspect, the original remote sensing image is decomposed by NSCT. The low-frequency component contains most of the image information and retains the characteristics of original image, whereas the high-frequency detail components are mixed with a great deal of noise. Thus, the low frequency component can serve as the input image of SURF algorithm. In terms of output aspect, after pre-matching two images through SURF algorithm, wrong matching point pairs are eliminated by using RANSAC algorithm (Fischler & Bolles, 1981).

The basic idea of RANSAC algorithm is presented below. A certain transform model between two images is assumed. Some matching point pairs are randomly selected to calculate the parameters of transform model. Then, the set of parameters are used to determine whether other matching point pairs conform to the transform model. After repeating the process numerous times, the set of parameters with the most matching point pairs is chosen to construct the true transform model. The transform relationship between two remote sensing images approximately meets the affine transformation model.

$$\begin{bmatrix} x_i' \\ y_i' \\ 1 \end{bmatrix} = \begin{bmatrix} a_1 & a_2 & a_3 \\ b_1 & b_2 & b_3 \\ 0 & 0 & 1 \end{bmatrix} \begin{bmatrix} x_i \\ y_i \\ 1 \end{bmatrix} \tag{4}$$

where a_1, a_2, a_3, b_1, b_2, and b_3 are affine transformation parameters. (x_i, y_i) refers to the coordinates of feature point in the image to be matched, and (x_i', y_i') denotes the coordinates of feature point in the reference image. Therefore, four sets of matching point pairs are substituted in Eq. (4), from which a set of transform model parameters can be obtained.

The process of the proposed algorithm is shown in Fig. 3. The algorithmic steps are enumerated below.

Step 1 The reference image and image to be matched are inputted.

Step 2 The reference image and image to be matched are decomposed by three layers of NSCT.

Step 3 The low-frequency components of two images decomposed by NSCT are regarded as the input images of SURF algorithm. Pre-matching is performed.

Step 4 Four sets of matching point pairs from the pre-matching results of SURF algorithm are randomly selected. Transformation matrix is calculated according to Eq. (4). All matching point pairs are traversed according to the obtained

transformation matrix. Then, percentage r under a certain threshold T is calculated, which meets the transformation matrix model.

Step 5 Step 4 is repeated N times ($N = 10000$ in this paper) and the matrix with the maximum r is selected as the correct transformation matrix.

Step 6 Matching point pairs with error larger than T under the transformation matrix are removed. Final matching results are obtained.

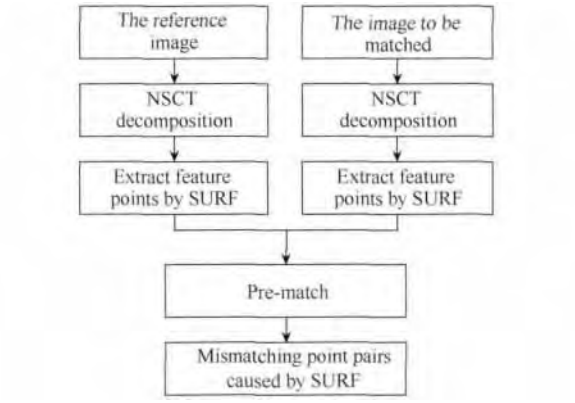

Fig. 3 Flowchart of the proposed algorithm

5 EXPERIMENTAL RESULTS AND ANALYSIS

To compare the proposed algorithm with the SIFT and SURF algorithms in terms of matching performance and various anti-interference capabilities in detail, a large number of experiments of the aforementioned algorithms on actual remote sensing images are conducted, and a quantitative evaluation and analysis are performed. The quantitative evaluation includes matching performance, anti-rotation capability, anti-noise capability, anti-brightness change capability, and anti-comprehensive interference capability analyses.

5.1 Matching performance analysis

Fig. 4 illustrates two remote sensing images which are different in size and angle at 236 × 168 and 192 × 153, respectively. Fig. 4(a) is matched with Fig. 4(b) by using the above mentioned algorithms. The number of extracted feature points, the number of matching point pairs, matching rate, and time consumed are shown in Table 1.

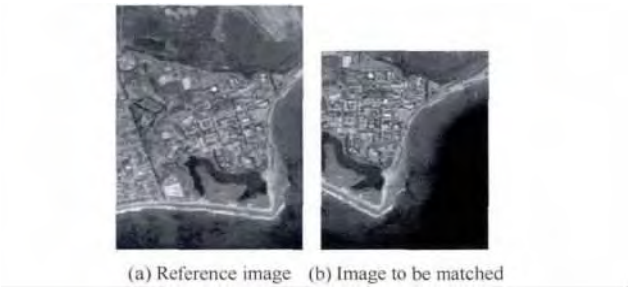

(a) Reference image (b) Image to be matched

Fig. 4 Remote sensing images

As shown in Table 1, the SIFT algorithm extracts the most number of feature points because the DoG that it adopts reflects the grayscale change of an image better than the box filter used by the SURF algorithm. The computational speed of SURF is almost three times higher than that of SIFT, but it has more wrong matching point pairs and has the lowest matching rate. The proposed algorithm has the highest speed, matching rate, and optimal performance.

Table 1 Comparisons of three algorithms in matching performance

	SIFT algorithm	SURF algorithm	Proposed algorithm
Number of feature points in reference image	450	212	184
Number of feature points in image to be matched	219	178	104
Number of pre-matching point pairs	72	43	56
Number of purified matching point pairs	69	29	43
Matching rate/%	31.5	16.3	41.3
Time consumed	3.12	1.08	0.82

5.2 Anti-rotation capability analysis

To test the anti-rotation capabilities of three algorithms, Fig. 4(b) is rotated at 0°, 45°, and 90°. Then, these three rotated images are matched with Fig. 4(a). The anti-rotation capabilities of three algorithms are analyzed, and the detailed comparison results are shown in Table 2.

Table 2 Comparisons of three algorithms in anti-rotation capability

Rotation angle/(°)	Algorithm	Number of feature points in reference image	Number of feature points in image to be matched	Number of pre-matching point pairs	Number of purified matching point pairs	Matching rate/%
0	SIFT	450	219	72	69	31.5
	SURF	212	178	43	29	16.3
	Proposed	184	104	56	43	41.3
45	SIFT	450	238	37	34	14.3
	SURF	212	351	25	16	7.5
	Proposed	184	262	44	36	23.9
90	SIFT	450	216	69	64	29.6
	SURF	212	174	44	28	16.3
	Proposed	184	101	58	43	42.6

As shown in Table 2, the three algorithms have similar anti-rotation capabilities, and the matching effect of 90° rotation is better than that of 45° rotation. After the image to be matched is rotated at 45°, the number of purified matching point pairs of the SIFT algorithm is reduced by 35, that of the SURF algorithm is reduced by 13, whereas that of the proposed algorithm is only reduced by seven. Therefore, the proposed algorithm is obviously superior to SIFT and SURF in terms of anti-rotation capability.

5.3 Anti-noise capability analysis

The Gaussian noise of different variances and salt and pepper noise of different noise density are added into Fig. 4(b), and then they are matched with Fig. 4(a). The comparisons of three algorithms in terms of anti-noise capability are shown in Fig. 5.

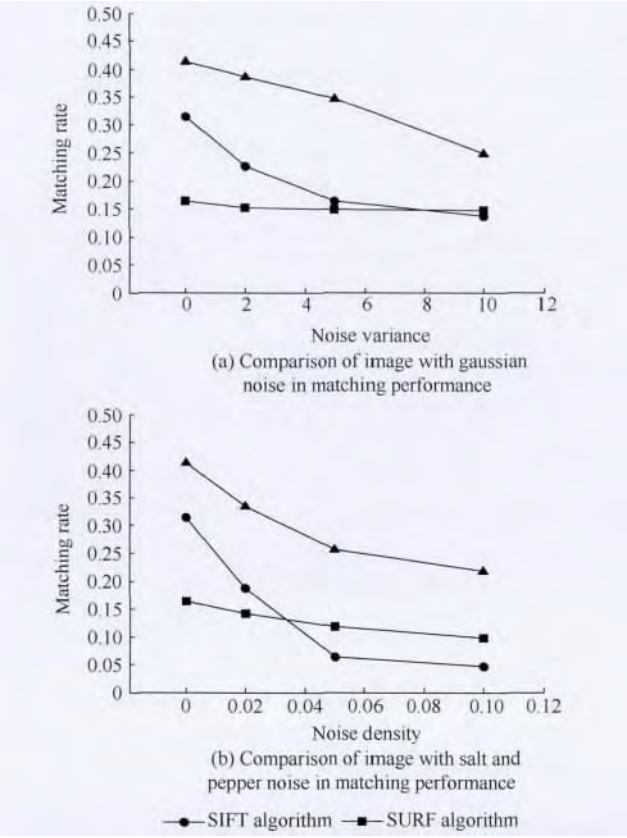

Fig. 5 Comparisons of three algorithms in anti-noise capability

As shown in Fig. 5, the matching rate of SURF algorithm is lower than that of the SIFT algorithm without noise. However, with increasing Gaussian noise variance/salt and pepper noise density, the matching rate of the SIFT algorithm decreases dramatically compared with that of SURF. Thus, its anti-noise capability is obviously inferior to that of the SURF algorithm. The anti-noise performance of the proposed algorithm is the best, and its matching rate is significantly higher than that of the other two algorithms because the low-frequency component after using NSCT decomposition basically retains the overall characteristics of the original image, whereas the high-frequency component reflects the image detail and contains the most noise. If the high-frequency component is also considered for matching, wrong matching results are frequently obtained because of the effect of high-frequency noise, and the matching time consumption is high. In this paper, only the low-frequency component of image is matched, which can significantly reduce the effect of noise and other details, thus accelerating the matching and improving its precision.

5.4 Anti-brightness change capability analysis

After processing Fig. 4(b), low, middle, and high brightness are constructed. Fig. 4(b) is the middle-brightness image. The low-brightness image is obtained through Fig. 4(b) with the brightness decreased by four times, and the high-brightness image is obtained by using Fig. 4(b) with the brightness increased two times. Fig. 4(a) is matched with three brightness images, and the anti-brightness change capabilities of three algorithms are analyzed. The detailed comparison results are shown in Table 3.

As shown in Table 3, when brightness is low, only the matching rate of the SIFT algorithm falls slightly, whereas the matching rate of the SURF and the proposed algorithms remains essentially unchanged. When brightness is high, the matching rate of the three algorithms all decrease. However, the matching rate of SIFT has the greatest decrease, followed by that of SURF. The anti-brightness change capability of the proposed algorithm is considered the best, followed by SURF algorithm, and the worst is the SIFT algorithm.

5.5 Anti-comprehensive interference capability analysis

To test the comprehensive interference capability of the three algorithms in terms of resistance to rotation, noise, and brightness change, Fig. 4(b) is rotated 45°, and the salt and pepper

Table 3 Comparisons of three algorithms in anti-brightness change capability

Brightness	Algorithm	Number of reference image feature points	Number of image to be matched feature points	Number of pre-matching point pairs	Number of purified matching point pairs	Matching rate/%
Middle	SIFT	450	219	72	69	31.5
	SURF	212	178	43	29	16.3
	Proposed	184	104	56	43	41.3
Low	SIFT	450	217	68	63	29.0
	SURF	212	178	41	30	16.8
	Proposed	184	99	57	44	44.4
High	SIFT	450	227	19	15	6.6
	SURF	212	190	32	11	5.8
	Proposed	184	111	40	26	23.4

noise with 0.1 noise density is added. Brightness is then reduced two times and finally matched with Fig. 4(a). The anti-comprehensive interference capabilities of three algorithms are analyzed, and the detailed comparison results are shown in Table 4.

As shown in Table 4, the matching rates of the three algorithms all have a large range of reductions after adding comprehensive interference. However, the matching rate of the SIFT a lgorithm is significantly influenced, followed by the SURF a lgorithm. The proposed algorithm has the best anti-comprehensive interference capability.

Table 4 Comparisons of three algorithms in anti-comprehensive interference capability

Image to be matched	Algorithm	Number of reference image feature points	Number of image to be matched feature points	Number of pre-matching point pairs	Number of purified matching point pairs	Matching rate/%
Original image	SIFT	450	219	72	69	31.5
	SURF	212	178	43	29	16.3
	Proposed	184	104	56	43	41.3
Image added with comprehensive interference	SIFT	450	541	6	5	1.1
	SURF	212	412	23	10	4.7
	Proposed	184	338	34	24	13.0

6 CONCLUSION

A remote sensing image matching algorithm based on NSCT and SURF is proposed. NSCT is used to decompose the reference image and the image to be matched. To reduce the i nfluence of high-frequency noise on matching results, the o btained low-frequency components of two images serve as the input images to be matched by the SURF algorithm. Finally, the RANSAC algorithm is used to eliminate the wrong matching point pairs. Experimental results show that the proposed algorithm is faster and has higher matching accuracy compared with the SIFT and SURF algorithms. The proposed algorithm is also significantly superior to the other algorithms in terms of anti-rotation, anti-noise, anti-brightness change, and anti-comprehensive interference capabilities.

REFERENCES

Bay H, Ess A, Tuytelaars T and Gool L V. 2008. Speeded-up robust features(SURF). Computer Vision and Image Understanding, 110(3): 346 – 359

Cunha A L, Zhou J P and Do M N. 2006. The nonsubsampled contourlet transform: theory, design, and applications. IEEE Transactions on Image Processing, 15(10): 3089 – 3101 [DOI: 10.1109/TIP.2006.877507]

Bouchafa S and Zavidovique B. 2006. Efficient cumulative matching for image registration. Image and Vision Computing, 24(1): 70 – 79 [DOI: 10.1016/j.imavis.2005.09.013]

Dufournaud Y, Schmid C and Horaud R. 2004. Image matching with scale adjustment. Computer Vision and Image Understanding, 93(2): 175 – 194

Fischler M A and Bolles R C. 1981. Random sample consensus: a paradigm for model fitting with applications to image analysis and automated cartography. Communications of the ACM, 24(6): 381 – 395

Ke Y and Sukthankar R. 2004. PCA-SIFT: a more distinctive representation for local image descriptors // Proceedings of the 2004 IEEE Computer Society Conference on Computer Vision and Pattern Recognition. Washington, DC: IEEE Computer Society

Li Q L, Wang G Y, Liu J G and Chen S. 2009. Robust scale-invariant feature matching for remote sensing image registration. IEEE Geoscience and Remote Sensing Letters, 6(2): 287 – 291 [DOI: 10.1109/LGRS.2008.2011751]

Li X M, Zheng L and Hu Z Y. 2006. SIFT based automatic registration of remotely-sensed imagery. Journal of Remote Sensing, 10(6): 885 – 892 [DOI: 10.3321/j.issn:1007 – 4619.2006.06.009]

Liu G X and Wang L. 2007. An image registration method based on region selecting and feature points matching. Journal of Optoelectronics · Laser, 18(8): 999 – 1002 [DOI: 10.3321/j.issn:1005 – 0086.2007.08.031]

Lowe D G. 2004. Distinctive image features from scale-invariant keypoint. International Journal of Computer Vision, 60(2): 91 – 110 [DOI: 10.1023/B:VISI.0000029664.99615.94]

Liu X J, Yang J, Sun J W and Liu Z. 2008. Image registration approach based on SIFT. Infrared and Laser Engineering, 37(1): 156 – 160

Liu Y, Wang J D and Li P. 2011. A feature point tracking method based on the combination of SIFT algorithm and KLT matching algorithm. Journal of Astronautics, 32(7): 1618 – 1625

Liang D, Yan P, Zhu M and Hu G S. 2011. Remote sensing image registration algorithm based on SIFT and NSCT. Chinese Journal of Scientific Instrument, 32(5): 1083 – 1088

Mikolajczyk K and Schmid C. 2005. A performance evaluation of local descriptors. IEEE Transactions on Pattern Analysis and Machine Intelligence, 27(10): 1615 – 1630 [DOI: 10.1109/TPAMI.2005.188]

Wang W and Zhao H R. 2011. The improvement of SUSAN for image matching. Journal of Remote Sensing, 15(5): 940 – 956

Wu J N, Guo B L and Feng Z Z. 2006. An image mosaic technique based on interest points feature matching. Journal of Optoelectronics · Laser, 17(6): 733 – 737 [DOI: 10.3321/j.issn:1005 – 0086.2006.06.021]

Wu J, Zhu C G and Zhao Z M. 2002. A novel method for rotation-invariant image matching based on wavelet analysis. Journal of Remote Sensing, 6(5): 339 – 342 [DOI: 10.3321/j.issn:1007 – 4619.2002.05.004]

Xue M G, Han Y S, Li C L, Yuan G L and Leng X Y. 2006. A new sequential frame image registration based on area homonymy matrix. Journal of Image and Graphics, 11(1): 53 – 59 [DOI: 10.3969/j.issn.1006 – 8961.2006.01.009]

Zhang P Q, Yu X C, Han L and Liu J Z. 2007. Automatic registration of images sequence based on line matching approach. Geomatics and Information Science of Wuhan University, 32(8): 676 – 679 [DOI: 10.3969/j.issn.1671 – 8860.2007.08.005]

Zhu Z W, Shen Z F and Luo J C. 2011. Parallel remote sensing image registration based on improved SIFT point feature. Journal of Remote Sensing, 15(5): 1024 – 1039

基于 NSCT 和 SURF 的遥感图像匹配

吴一全[1,2,3],沈毅[1],陶飞翔[1]

1. 南京航空航天大学 电子信息工程学院,江苏 南京 210016;
2. 农业部农业信息技术重点实验室,北京 100081;
3. 江西省数字国土重点实验室,江西 南昌 330013

摘 要:SURF(Speed Up Robust Features)算法是对尺度不变特征变换 SIFT(Scale Invariant Feature Transform)算法的一种改进,应用到遥感图像匹配领域中可以大大提高匹配速度,但是匹配精度略有下降。为此,本文提出一种基于无下采样 Contourlet 变换 NSCT(Nonsubsampled Contourlet Transform)和 SURF 的遥感图像匹配算法。首先使用 NSCT 分别分解参考图像和待匹配图像,得到各自对应的低频分量;然后把这两幅低频分量图像作为 SURF 算法的输入图像进行预匹配,降低高频噪声对匹配结果的影响;最后利用预匹配结果求解变换模型的参数,并采用随机抽样一致 RANSAC (Random Sample Consensus)算法剔除误匹配点对,解决了 SURF 算法存在的错误匹配问题。实验结果表明,与 SIFT 算法、SURF 算法相比,本文算法具有更高的匹配精度和更快的匹配速度,且抗旋转、噪声、亮度变化能力更强。

关键词:遥感图像匹配,尺度不变特征变换,SURF 算法,无下采样 Contourlet 变换(NSCT)

中图分类号:TP751.1 **文献标志码**:A

引用格式:吴一全,沈毅,陶飞翔. 2014. 基于 NSCT 和 SURF 的遥感图像匹配. 遥感学报,18(3):618-629

Wu Y Q, Shen Y and Tao F X. 2014. Remote sensing image matching based on non-subsampled contourlet transform and speed up robust features. Journal of R emote Sensing, 1 8(3): 618-629 [DOI: 10.11834/jrs.20143113]

1 引 言

图像匹配是指将两幅或多幅图像进行比较,找到它们的共有景物,或者根据已知目标图像到未知目标图像中寻找相应的特定目标。它广泛应用于计算机视觉、医学图像分析和飞行器巡航制导等诸多领域。在遥感图像处理中,图像匹配最重要的应用之一就是对遥感图像的配准。图像配准是图像融合、变化检测的基本预处理步骤,配准精度对后续数据的处理具有重要的影响。人们对图像匹配已进行了大量的研究,现有的图像匹配算法大致可分为基于灰度的匹配和基于点(Dufournaud 等,2004;仵建宁 等,2006;王巍和赵红蕊,2011)、线(Bouchafa 和 Zavidovique,2006;张鹏强 等,2007)、区域(薛模根等,2006;刘贵喜和王蕾,2007)等特征(吴均 等,2002)的匹配两类算法。由于拍摄时间和拍摄环境不同,同一场景的遥感图像之间灰度可能相差较大,基于灰度的匹配算法可能得不到很好的效果,且受噪声的影响很大。而基于特征的匹配算法通过提取两幅图像的共同特征来实现,在提取特征的过程中可以减少噪声的影响,更适合遥感图像的匹配。Lowe(2004)总结了现有的基于不变量技术的特征检测算法,提出一种尺度不变特征变换 SIFT(Scale Invariant Feature Transform)算法。基于尺度空间的 SIFT 算子对图像旋转、缩放甚至仿射变换保持不变,被广泛应用于遥感图像匹配中(李晓明 等,2006;刘小军 等,2008;Li 等,2009;刘玉 等,2011;朱志文 等,2011)。为了抑制高频噪声的影响,梁栋等人(2011)将多分辨率分析和 SIFT 算法综合起来,在一定程度上提高了运算速度和匹配精度。然而,由

收稿日期:2013-05-09;修订日期:2013-11-08;优先数字出版日期:2013-11-15

基金项目:国家自然科学基金(编号:60872065);农业部农业科研杰出科技人才基金和农业部农业信息技术重点实验室开放基金(编号:2013001);江西省数字国土重点实验室开放基金(编号:DLLJ201113);江苏高校优势学科建设工程资助项目

第一作者简介:吴一全(1963—),男,博士,教授,主要研究方向为遥感图像处理、分析与理解和目标检测与识别等。已在国内外核心期刊发表学术论文 200 余篇。E-mail:nuaaimage@163.com

于 SIFT 算法存在着描述符维数过高、检测和匹配速度慢以及对视角变化较敏感等缺点，很难满足对实时性要求很高的场合。PCA-SIFT（Ke 和 Sukthankar，2004）和 GLOH（Mikolajczyk 和 Schmid，2005）等改进算法被相继提出，但效果不太理想。2006 年，借鉴了 SIFT 算法中简化近似的思想，Bay 等人（2008）引入积分图像并将高斯二阶微分模板进行了近似简化，提出了 SURF（Speeded Up Robust Features）算法。与 SIFT 算法相比，SURF 算法在速度上要快 3 倍左右，但是错误匹配点较多。

针对 SURF 算法在速度上的优势和其错误匹配点对较多的缺点，提出一种基于无下采样 Contourlet 变换 NSCT（Nonsubsampled Contourlet Transform）和 SURF 的遥感图像匹配算法。首先使用 NSCT 分别对参考图像和待匹配图像进行分解，得到包含大量原始图像信息的低频分量图像；然后把两幅低频分量图像作为 SURF 算法的输入图像进行预匹配，降低高频噪声对匹配结果的影响；再根据预匹配结果求解变换模型的参数，并采用随机抽样一致 RANSAC（Random Sample Consensus）算法剔除预匹配中还存在的错误匹配点对；最后通过实验与 SIFT、SURF 算法进行比较，综合分析本文算法的各种抗干扰能力，验证本文算法的优越性。

2 NSCT 算法

Contourlet 变换使用塔形方向滤波器组分解图像，其过程可分为子带分解和方向变换两个阶段。子带分解阶段利用拉普拉斯塔式分解将每层低频分量分解成 1 个低频分量和 1 个高频分量，方向变换阶段利用方向滤波器组将高频分量分解成 2^i 个方向子带（i 为正整数），由此可得到图像的多尺度多方向分解。但 Contourlet 变换的分解中存在下采样过程，系数冗余度大大降低，却无平移不变性，图像处理结果会产生振铃现象。此外，在实现 Contourlet 变换时，分析滤波器和综合滤波器的带宽都大于 $\pi/2$，不满足采样定理，导致低频分量和高频分量存在频谱混叠现象。由无下采样塔式分解 NSP（Nonsubsampled Pyramid）和无下采样方向滤波器组 NSDFB（Nonsubsampled Directional Filter Bank）构成的 NSCT（Cunha 等，2006）可以解决这一问题。对于每一层来说，NSP 先将上一层的低频分量分解为高频和低频两个分量，然后 NSDFB 再将高频分量分解为多个方向子带。NSCT 分解示意图如图 1 所示。NSCT 与 Contourlet 变换的差别是：NSCT 消除了 Contourlet 变换的频谱混淆现象，在图像分解及重构的过程中，它对 NSP 和 NSDFB 分解所得的各信号分量没有应用分析滤波之后的下采样及综合滤波之前的上采样，而是先对相应滤波器进行上采样，再对信号进行分析滤波和综合滤波。因此，NSCT 不仅具有多尺度、局部性和多方向等特性，还具有平移不变性及各子带图像均具有相同尺寸的特点。

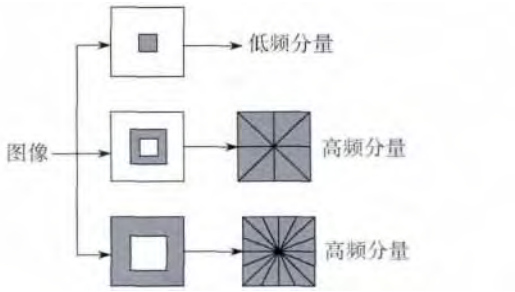

图 1 NSCT 分解示意图

3 SURF 算法

SURF 算法是 SIFT 算法的改进算法，它具有对于尺度变化和旋转的鲁棒性，且速度更快。算法包括特征点检测、特征点描述和特征点匹配 3 个部分。

3.1 特征点检测

SIFT 利用对前层图像下采样得到后层图像，然后与不同尺度的高斯内核卷积，对相邻层求差，从而得到 DoG（Difference of Gaussians）空间，最后通过寻找 DoG 空间的局部极值点来检测特征点。为了提高速度，SURF 并不对图像下采样，而是利用盒子滤波来近似高斯滤波，然后不断增大盒子滤波模板尺寸并与积分图像共同求取 Hessian 矩阵行列式的响应函数，再在响应函数上通过非极大值抑制法求取特征点。

对于图像 I 中某点 $X(x,y)$，在 X 点的尺度 σ 上的 Hessian 矩阵定义为

$$\boldsymbol{H}(X,\sigma)=\begin{bmatrix}L_{xx}(X,\sigma) & L_{xy}(X,\sigma)\\ L_{xy}(X,\sigma) & L_{yy}(X,\sigma)\end{bmatrix} \quad (1)$$

式中，$L_{xx}(X,\sigma)$、$L_{xy}(X,\sigma)$ 和 $L_{yy}(X,\sigma)$ 表示点 X 处二阶高斯滤波与图像的卷积。

Bay 等人（2008）提出可以使用盒子滤波来近似高斯滤波，卷积过程的计算量则与滤波器大小无关，如图 2 所示。Hessian 矩阵行列式的近似过程为

$$\mathrm{Det}(\boldsymbol{H})=L_{xx}L_{yy}-L_{xy}^2=D_{xx}D_{yy}-(0.9D_{xy})^2 \quad (2)$$

式中,D_{xx}、D_{yy}和D_{xy}分别是图2中近似后的模板与图像卷积的结果;0.9为权重系数,主要是为了平衡近似误差,Bay指出它对实验结果没有显著影响。

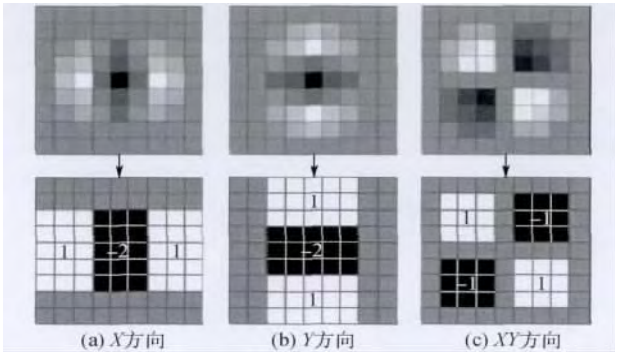

图2 高斯二阶导数的近似表示

另外,为了进一步提高计算速度,可以使用积分图像完成图像卷积操作,积分图像$I_{\Sigma}(X)$定义为以点X和图像原点为对角顶点所形成矩形区域内的像素值之和,即

$$I_{\Sigma}(X)=\sum_{i=0}^{x}\sum_{j=0}^{y}I(i,j) \tag{3}$$

计算积分图像时,只需要遍历1次原图像,计算量很小。

3.2 特征点描述

SIFT使用特征点邻域的梯度信息进行特征点描述,而SURF使用的是特征点邻域的灰度信息,通过计算积分图像的一阶Haar小波响应,得到灰度分布信息来产生特征点描述向量。

步骤1 主方向分配:在特征点的半径为6σ(σ为特征点所在尺度)的圆形邻域计算x和y方向上的Haar小波响应系数,然后将60°范围内的响应相加形成新的向量,遍历整个圆形区域后选择最长向量的方向作为该特征点的主方向。

步骤2 生成特征向量:将坐标轴旋转为特征点的主方向,以确保旋转不变性,然后将其周围20σ的正方形区域划分为4×4个子域,对每个子域计算5×5个采样点的Haar小波响应。假定dx表示水平方向上Haar小波响应,dy表示垂直方向上Haar小波响应,则子域可以表示为$v=[\sum dx,\sum dy,\sum|dy|,\sum|dy|]$,所有子域的向量就串接成该特征点的64维特征向量。

3.3 特征点匹配

常用的特征匹配算法:对于某一特征向量,首先计算另一图像中所有特征向量与该向量的距离,然后求最近邻与次近邻的比值,如果比值小于预先设定的阈值,则认为该最近邻是较好的匹配。

4 基于NSCT和SURF的遥感图像匹配算法原理

SURF算法虽然可以大幅提高SIFT的运算速度,但是错误匹配点对较多。为了解决这一问题,本文提出一种基于NSCT和SURF的遥感图像匹配算法,分别从输入和输出两个方面提高匹配性能。在输入方面,利用NSCT分解原始遥感图像,由于低频分量包含了图像的大部分信息,基本保持了原始图像的特征,而高频细节分量却夹杂了许多噪声,因此可以将低频分量作为SURF算法的输入图像;在输出方面,在通过SURF算法对两幅图像预匹配后,采用RANSAC算法(Fischler和Bolles,1981)剔除误匹配点对。

RANSAC算法的基本思想是,假定两幅图像之间存在某种变换模型,每次随机选取一些匹配点对计算出该模型的参数,再利用这组参数去判断其他匹配点对是否符合该变换模型,重复多次后,选取匹配点对最多的那组参数构建真正的变换模型。遥感图像之间的变换近似满足仿射变换模型

$$\begin{bmatrix}x_i'\\y_i'\\1\end{bmatrix}=\begin{bmatrix}a_1&a_2&a_3\\b_1&b_2&b_3\\0&0&1\end{bmatrix}\begin{bmatrix}x_i\\y_i\\1\end{bmatrix} \tag{4}$$

式中,a_1、a_2、a_3、b_1、b_2和b_3为仿射变换参数,(x_i,y_i)表示待匹配图像特征点的坐标,(x_i',y_i')为表示参考图像特征点的坐标。因此,每次将4组匹配点对代入式(4),即可求解出一组变换模型参数。

综上所述,本文算法流程如图3所示,算法步骤描述如下:

步骤1 输入参考图像和待匹配图像。

步骤2 分别对参考图像和待匹配图像进行NSCT分解(本文做3层分解)。

步骤3 对NSCT分解后的低频分量图像利用SURF算法提取特征点并进行预匹配。

步骤4 从SURF算法预匹配中随机选取4组匹配点对,按式(4)计算出变换矩阵,并根据得到的变换矩阵遍历所有匹配点对,计算在某个特定的阈值T下满足该变换矩阵模型的百分比r。

步骤5 重复步骤4共n次(本文n取10000),取r最大的矩阵作为正确的变换矩阵。

步骤 6 将在该变换矩阵下误差超过 T 的匹配点对去除，得到最终的匹配结果。

图 3 算法流程图

5 实验结果与分析

为了详细比较 SIFT 算法、SURF 算法和本文算法的匹配性能和各种抗干扰能力，分别采用上述 3 种算法，针对实际的遥感图像做了大量的实验并进行了定量评价与分析。具体包括：匹配性能分析、抗旋转能力分析、抗噪声能力分析、抗亮度变化能力分析以及抗综合干扰能力分析。

5.1 匹配性能分析

图 4 是两幅尺寸不同且存在角度差异的遥感图像，大小分别为 236×168 和 192×153。分别利用 3 种算法对图 4(a) 和图 4(b) 进行匹配，提取特征点数、匹配点对数、匹配率及耗时分析见表 1。表 1 中匹配率是提纯后的匹配点对数与待匹配图特征点数的比值。

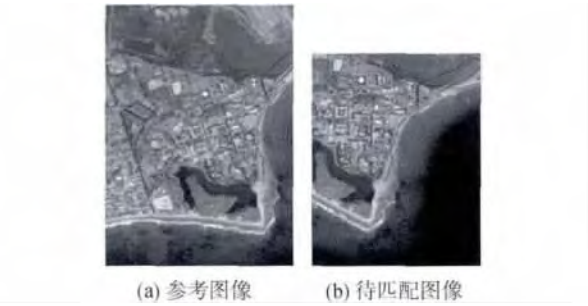

图 4 遥感图像

由表 1 可知，SIFT 算法提取的特征点数最多，这是由于 SIFT 所采用的 DoG 比 SURF 所采用的盒式滤波器更能反映图像的灰度变化；SURF 算法的计算速度比 SIFT 算法提高了将近 3 倍，但是误匹配点对较多，匹配率最低；本文算法速度最快，匹配率最高，性能最优。

表 1 3 种算法的匹配性能对比

	SIFT 算法	SURF 算法	本文算法
参考图像特征点数	450	212	184
待匹配图像特征点数	219	178	104
预匹配点对数	72	43	56
提纯后匹配点对数	69	29	43
匹配率/%	31.5	16.3	41.3
耗时/s	3.12	1.08	0.82

5.2 抗旋转能力分析

为了检测 3 种算法的抗旋转能力，将图 4(b) 分别旋转 0°，45° 和 90°，然后将图 4(a) 分别与 3 幅旋转后的待匹配图像进行匹配，分析 3 种算法的抗旋转能力，详细对比结果见表 2。

表 2 3 种算法的抗旋转能力对比

旋转角度/(°)	算法	参考图像特征点数	待匹配图像特征点数	预匹配点对数	提纯后匹配点对数	匹配率/%
0	SIFT 算法	450	219	72	69	31.5
	SURF 算法	212	178	43	29	16.3
	本文算法	184	104	56	43	41.3
45	SIFT 算法	450	238	37	34	14.3
	SURF 算法	212	351	25	16	7.5
	本文算法	184	262	44	36	23.9
90	SIFT 算法	450	216	69	64	29.6
	SURF 算法	212	174	44	28	16.3
	本文算法	184	101	58	43	42.6

由表 2 可以看出，3 种算法的抗旋转能力相差不大，且对旋转 90° 的图像匹配效果优于旋转 45° 的图像。待匹配图像旋转 45° 后，SIFT 算法得到的提纯后匹配点对减少了 35 对，SURF 算法减少了 13 对，本文算法只减少了 7 对。可见，本文算法的抗旋转能力明显优于 SIFT 算法和 SURF 算法。

5.3 抗噪声能力分析

分别将不同方差的高斯噪声和不同噪声密度的椒盐噪声加入图4(b)中,然后与图4(a)进行匹配,3种算法的抗噪声能力对比如图5所示。

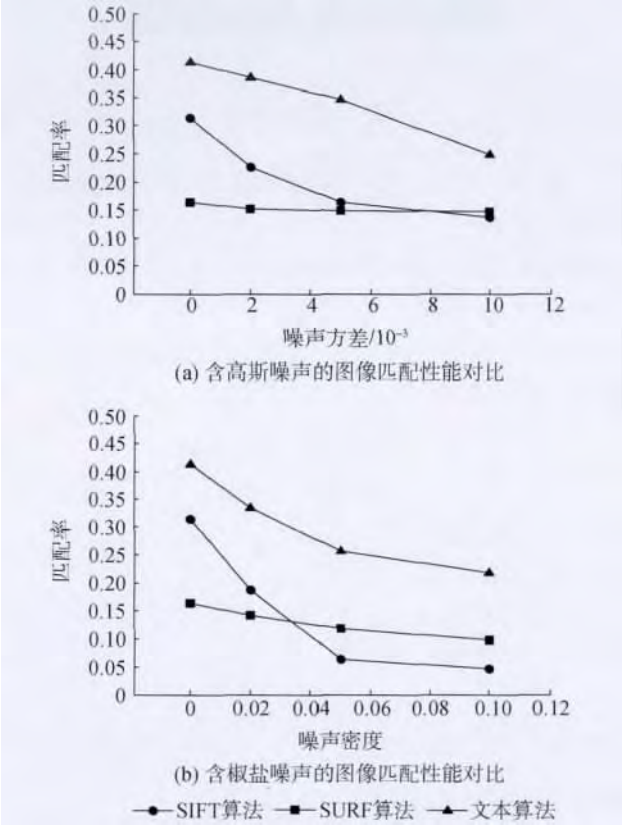

图5 3种算法的抗噪声能力对比

由图5可知,虽然在不含噪声的情况下,SURF算法的匹配率低于SIFT算法,但是随着高斯噪声方差/椒盐噪声密度的增加,SIFT算法的匹配率在大幅下降,幅度远高于SURF算法,抗噪能力明显不如SURF算法;而本文算法抗噪性能最好,匹配率始终比其他两种算法有绝对优势。这是因为利用NSCT分解图像后,低频分量基本保持了原图的整体特征,而高频分量反映了图像的细节,含有大部分的噪声,如果匹配的时候把高频分量也考虑进去,不但常常受高频噪声的影响而产生误匹配,而且匹配分析的时间消耗也很大。本文只对图像低频分量进行匹配,可以大大降低噪声等细节的影响,使得算法既加快了匹配的速度也提高了匹配的精度。

5.4 抗亮度变化能力分析

对图4(b)处理,构造低、中、高3种不同亮度。其中,图4(b)就是中亮度图像,低亮度图像由图4(b)将亮度降低4倍所得,高亮度图像为图4(b)将亮度提高2倍所得。然后将图4(a)分别与这3种亮度图像进行匹配,分析3种算法的抗亮度变化能力,详细对比结果见表3。

由表3可知,当亮度较低的时候,只有SIFT算法的匹配率略有下降,SURF算法和本文算法基本不变;当亮度较高的时候,3种算法的匹配率都有所降低,但SIFT算法下降幅度最大,SURF算法次之。由此可以得出:本文算法抗亮度变化性能最好,SURF算法次之,SIFT算法最差。

表3 3种算法的抗亮度变化能力对比

亮度	算法	参考图像特征点数	待匹配图像特征点数	预匹配点对数	提纯后匹配点对数	匹配率/%
中	SIFT算法	450	219	72	69	31.5
	SURF算法	212	178	43	29	16.3
	本文算法	184	104	56	43	41.3
低	SIFT算法	450	217	68	63	29.0
	SURF算法	212	178	41	30	16.8
	本文算法	184	99	57	44	44.4
高	SIFT算法	450	227	19	15	6.6
	SURF算法	212	190	32	11	5.8
	本文算法	184	111	40	26	23.4

5.5 抗综合干扰能力分析

为了测试3种算法抗旋转、噪声和亮度变化综合干扰的能力,先将图4(b)旋转45°,然后加入噪声密度为0.1的椒盐噪声,再将亮度降低2倍,最后与图4(a)做匹配,分析3种算法抗综合干扰的能力,详细对比结果见表4。

表 4 3 种算法的抗综合干扰能力对比

待匹配图像	算法	参考图像特征点数	待匹配图像特征点数	预匹配点对数	提纯后匹配点对数	匹配率/%
原图	SIFT 算法	450	219	72	69	31.5
	SURF 算法	212	178	43	29	16.3
	本文算法	184	104	56	43	41.3
加入综合干扰后的图像	SIFT 算法	450	541	6	5	1.1
	SURF 算法	212	412	23	10	4.7
	本文算法	184	338	34	24	13.0

由表 4 可知，加入综合干扰后，3 种算法的匹配率都有了很大幅度的下降，但 SIFT 算法受到影响最大，SURF 算法次之，本文算法的抗综合干扰能力最强。

6 结 论

提出一种基于 NSCT 和 SURF 的遥感图像匹配算法。首先利用 NSCT 分别分解参考图像和待匹配图像；然后把各自得到的低频分量作为 SURF 的输入图像进行匹配，抑制了高频噪声的影响；最后使用 RANSAC 算法去除误匹配点对。实验结果表明，与 SIFT 算法和 SURF 算法相比，本文算法的运算速度更快，匹配精度更高，且无论是抗旋转能力、抗噪声能力、抗亮度变化能力，还是抗综合干扰能力，本文算法都明显优于其他两种算法。

参考文献(References)

Bay H, Ess A, Tuytelaars T and Gool L V. 2008. Speeded-up robust features(SURF). Computer Vision and Image Understanding, 110(3): 346 – 359

Cunha A L, Zhou J P and Do M N. 2006. The nonsubsampled contourlet transform: theory, design, and applications. IEEE Transactions on Image Processing, 15(10): 3089 – 3101 [DOI: 10.1109/TIP.2006.877507]

Bouchafa S and Zavidovique B. 2006. Efficient cumulative matching for image registration. Image and Vision Computing, 24(1): 70 – 79 [DOI: 10.1016/j.imavis.2005.09.013]

Dufournaud Y, Schmid C and Horaud R. 2004. Image matching with scale adjustment. Computer Vision and Image Understanding, 93(2): 175 – 194

Fischler M A and Bolles R C. 1981. Random sample consensus: a paradigm for model fitting with applications to image analysis and automated cartography. Communications of the ACM, 24(6): 381 – 395

Ke Y and Sukthankar R. 2004. PCA-SIFT: a more distinctive representation for local image descriptors // Proceedings of the 2004 IEEE Computer Society Conference on Computer Vision and Pattern Recognition. Washington, DC: IEEE Computer Society

Li Q L, Wang G Y, Liu J G and Chen S. 2009. Robust scale-invariant feature matching for remote sensing image registration. IEEE Geoscience and Remote Sensing Letters, 6(2): 287 – 291 [DOI: 10.1109/LGRS.2008.2011751]

李晓明，郑链，胡占义. 2006. 基于 SIFT 特征的遥感影像自动配准. 遥感学报，10(6): 885 – 892 [DOI: 10.3321/j.issn:1007 – 4619.2006.06.009]

刘贵喜，王蕾. 2007. 基于区域选择和特征点匹配的图像配准算法. 光电子·激光，18(8): 999 – 1002 [DOI: 10.3321/j.issn:1005 – 0086.2007.08.031]

Lowe D G. 2004. Distinctive image features from scale-invariant keypoint. International Journal of Computer Vision, 60(2): 91 – 110 [DOI: 10.1023/B:VISI.0000029664.99615.94]

刘小军，杨杰，孙坚伟，刘志. 2008. 基于 SIFT 的图像配准方法. 红外与激光工程，37(1): 156 – 160

刘玉，王敬东，李鹏. 2011. 一种基于 SIFT 和 KLT 相结合的特征点跟踪方法研究. 宇航学报，32(7): 1618 – 1625

梁栋，颜普，朱明，胡根生. 2011. 一种基于 NSCT 和 SIFT 的遥感图像配准算法. 仪器仪表学报，32(5): 1083 – 1088

Mikolajczyk K and Schmid C. 2005. A performance evaluation of local descriptors. IEEE Transactions on Pattern Analysis and Machine Intelligence, 27(10): 1615 – 1630 [DOI: 10.1109/TPAMI.2005.188]

王巍，赵红蕊. 2011. 面向影像匹配的 SUSAN 角点检测. 遥感学报，15(5): 940 – 956

仵建宁，郭宝龙，冯宗哲. 2006. 一种基于兴趣点特征匹配的图像镶嵌技术. 光电子·激光，17(6): 733 – 737 [DOI: 10.3321/j.issn:1005 – 0086.2006.06.021]

吴均，朱重光，赵忠明. 2002. 一种基于小波分析的旋转不变图像快速匹配方法. 遥感学报，6(5): 339 – 342 [DOI: 10.3321/j.issn:1007 – 4619.2002.05.004]

薛模根，韩裕生，李从利，袁广林，冷晓艳. 2006. 基于区域同名度矩阵的连续帧图像配准. 中国图象图形学报，11(1): 53 – 59 [DOI: 10.3969/j.issn.1006 – 8961.2006.01.009]

张鹏强，余旭初，韩丽，刘景正. 2007. 基于直线特征匹配的序列图像自动配准. 武汉大学学报·信息科学版，32(8): 676 – 679 [DOI: 10.3969/j.issn.1671 – 8860.2007.08.005]

朱志文，沈占锋，骆剑承. 2011. 改进 SIFT 点特征的并行遥感影像配准. 遥感学报，15(5): 1024 – 1039